PHYSICS AND CHEMISTRY OF SOLID STATE
V. 27, No. 2 (2026) pp. 242-252

Section: Technology

DOI: 10.15330/pcss.27.2.242-252

Vasyl Stefanyk Carpathian National University

ФІЗИКА І ХІМІЯ ТВЕРДОГО ТІЛА
Т. 27, № 2 (2026) С. 242-252

Технічні науки

PACS: 82.45.Bb

ISSN 1729-4428 (Print)
ISSN 2309-8589 (Online)

Lochan Sharma[1], Amman Jakhar[2], Kanika Sharma[3], Mukhtiar Singh[4], Mandeep Singh Rayat[4], Mariia Liaskovska[5], Rashad Abaszade[6,7,8,9]

Investigation of microstructure, corrosion, and mechanical properties of MIG welded API X70 and SS401 joints

[1]Faculty of University Center of Research & Development, Chandigarh University, Mohali-140413, Punjab, India;
[2]Faculty of Mechanical Engineering Department, Chandigarh University, Mohali-140413, Punjab, India;
[3]Faculty of Computer Science and Engineering Department, Chandigarh University, Mohali-140413, Punjab, India;
[4]Lovely Professional University Jalandhar - Delhi, Grand Trunk Rd, Phagwara, Punjab, India;
[5]Department of Biological and Medical Chemistry named after Academician G.O. Babenko,
Ivano-Frankivsk National Medical University, Ivano-Frankivsk, Ukraine;
[6]Department of Electronics and Automatics, Azerbaijan State Oil and Industry University, Baku, Azerbaijan,
abaszada@gmail.com;
[7]Department of Ecology, Azerbaijan University of Architecture and Construction, Baku, Azerbaijan;
[87]Department of Materials Science and New Materials Technologies,
Tashkent State Technical University named after Islam Karimov, Tashkent, Uzbekistan;
[9]Electrical and Electronics Engineering Department, Turan International Research Institute, Baku, Azerbaijan

In present study, Metal Inert Gas (MIG) welding with ER309L austenitic filler wire was used to weld API X70 and SS 401 steel. This particular joint is mainly used in oil and gas plants where stainless steel need to be connected to the high strength low alloy carbon steel pipelines. MIG welding process is cost effective in these industrial fabrication and maintenance applications as it has high deposition rates and productivity. The investigation focuses on the influence of two distinct heat input levels-HI-1 (0.814 kJ/mm) and HI-2 (0.573 kJ/mm) on the weldment's microstructure, mechanical performance, and corrosion resistance in simulated seawater and sodium thiosulphate environments. Microstructural examination revealed that the lower heat input (HI-2) produced coarser grains and reduced martensite-austenite (MA) constituent formation in the fusion zone, resulting in improved toughness. Conversely, the higher heat input (HI-1) led to finer grains but increased brittleness. In the heat-affected zone (HAZ), API X70 exhibited grain coarsening-induced softening, while SS 401 demonstrated sensitization and MA phase development, negatively affecting corrosion resistance. Corrosion assessments indicated superior performance of SS 401 over API X70, with minimal weight loss (0.75 mm/year) in seawater due to its protective chromium-rich passive film. However, the dissimilar welded joints, particularly those produced with HI-1-showed significant corrosion degradation (2.1 mm/year in thiosulphate solution), primarily due to microstructural inhomogeneity and galvanic coupling. Mechanical testing results showed that HI-2 welds offered enhanced impact toughness (196 J in the fusion zone) compared to HI-1 (154 J), although the API X70 HAZ under HI-2 exhibited decreased toughness (120 J) likely due to thermal softening. Hardness measurements revealed maximum values near the fusion boundary (~380 HV in HI-1 samples), with noticeable softening in the HAZ regions. These findings suggest that optimizing heat input is critical for balancing mechanical integrity and corrosion resistance in dissimilar metal joints.

Keywords: Metal Welding, X70, SS401, HAZ, Fusion Zone, Corrosion Resistance, Microstructure, Fractography.

Received 26 November 2025; Accepted 03 April 2026; Published 16 April 2026.

Introduction

API 5L X70 gained popularity within hydrocarbon transportation pipelines because of its impressive strength performance and durable characteristics for challenging service conditions that extend to offshore infrastructure as well as seismic regional locations and arctic locations [1].

The substance finds its applications in construction projects and mining operations and heavy equipment production facilities that need high mechanical performance [2]. Scientists have researched improved corrosion protection through submerged arc welding (SAW) as an applied process [3]. The studies have explored both the vulnerability to hydrogen embrittlement and how severe cold rolling affects hydrogen permeation while modifying microstructure properties [4]. Researchers have examined how thermomechanical controlled processing affects the microstructure of the steel material [5]. The application of rare earth compounds serves as potential corrosion inhibitors for this steel grade as introduced in recent research [6]. The welding properties and average mechanical properties of ferritic stainless-steel SS 401 work well to support bridge and building structures and marine conditions when the steel is connected to steels from the API X-series [7]. Multiple hybrid designs benefit from better corrosion resistance due to the integration of these steel types. High-strength low-alloy (HSLA) and stainless steels join SS 401 to make automotive frames and chassis which excel at resistance to both strength demands and vehicle collision impacts [8]. High-pressure pipelines and refinery equipment within the oil and gas industry utilize SS 401 along with abrasion-resistant steels to enhance their wear properties until the railway sector employs them for similar applications [9]. SS 401 finds its use in power generation units through applications in boilers and turbines requiring welds between the material and heat-resistant alloys to achieve better fatigue performance [10]. In marine construction operations SS 401 works together with galvanized and marine-grade steels to defend against both corrosion and structural degradation of hulls and offshore platforms [11]. The welding of API 5L X70 alongside SS 401 presents demanding conditions because of the contrasting thermal performance and material chemical content along with material strength attributes. The main weld-related issues stem from brittle intermetallic appearances in fusion zones and the formation of coarse grains in the heat-affected zone that diminishes ductility [12]. The microstructure in fusion zone adopts its form based on fusion technique as well as from how rapidly the metal cools down [13]. The weld process utilizes GMAW and EBW technologies to overcome these problems [14]. Temperature management combined with initial heating and post-welding thermal treatment positions as key factors to minimize welding deficiencies and unwanted stresses and cracking occurrences [15]. The mechanical soundness of dissimilar welds between these steels requires precise welding parameter control according to [16]. Researchers address industrial requirements to develop sound welding techniques between dissimilar materials including API 5L X70 and SS 401 which serve in various pipeline implementations and offshore infrastructure and marine settings. The assessment of heat input effects on weld quality plus structural behavior together with corrosion performance must be studied to reach optimal weld parameters. The obtained knowledge enables durable performance combined with safety in conditions requiring high mechanical strength levels and excellent corrosion protection.

I. Experimental details

This research used API X70 along with SS 401 as the fundamental material selection. Both API X70 plate from Jindal Stainless Limited started at 300 mm × 300 mm × × 25 mm and SS 401 plate began with 500 mm × × 200 mm × 12 mm dimensions. The materials underwent spectrographic testing for determining their chemical compositions which generated the findings presented in Table 1. Welding operations used two specimens with dimensions 75 mm × 75 mm × 12 mm which were extracted from each base plate. A milling cutter produced precise geometrical chamfered edges on the specimens before machining. A 60-degree V-groove shaped joint was designed into the plate edges to improve welding penetration and weld fusion. A 2 mm gap served as the root distance during the process. Metal Inert Gas (MIG) welding was used to fuse ER309L filler wire with 1.2-millimeter diameter while using 1 bar argon shielding gas at 12 liters per minute (LPM) flow rate. The initial preparations included using a wire brush to clean each plate surface for complete removal of surface rust and debris alongside contaminants before welding. Acetone application facilitated strong bonding of filler wire to base metal by removing all remaining grease or oil residues from the surface. The cleaning approach became essential for reducing weld defects together with maintaining proper metallurgical connection. The materials received preheating treatment at 200°C. The thermal treatment minimized both weld zone stress and improved penetration and minimized cracking while controlling cooling rates specifically for enhancing thicker section welds. To maintain precise alignment and prevent displacement during welding, the specimens were clamped securely using a dedicated fixture. This setup ensured joint stability, contributing to uniform and consistent weld bead formation. Dissimilar weld joint between API X70 and SS401 is shown in Figure 1. The heat input for the welding process was determined using Eq. 1.

$$HI = (V \times I \times 60)/(S \times \eta) \qquad (1)$$

where HI represents heat input per unit length, V is the voltage (in volts), I is the welding current (in amperes), S is the welding speed (in mm/sec), and η denotes the thermal efficiency, set at 0.9 in this case. Two different heat input levels were employed: 0.814 kJ/mm (HI-1) and 0.573 kJ/mm (HI-2). These values significantly influenced the weld characteristics, including the microstructure, heat-affected zone (HAZ), and overall mechanical performance. A higher heat input generally results in a wider HAZ, lower hardness, and greater distortion. Conversely, lower heat input tends to produce stronger joints with improved dimensional control and microstructural refinement.

Charpy V-notch specimens were prepared in accordance with standardized testing protocols, such as ASTM E23 standard. Each specimen was precisely fabricated to feature a 45° notch angle, a notch depth of 2 mm, and a root radius of 0.25 mm. Vickers microhardness testing was also carried out to evaluate the hardness distribution across the weld metal and the heat-affected zone (HAZ). This test used a 0.5 kgf load with a dwell time of 20 seconds to ensure accurate measurements. The microstructural characterization process involved a sequence of polishing, etching, and microscopic observation. Initial surface preparation began with polishing using abrasive papers of progressively finer grit, starting from 120 grit and moving through 150, 250, 400, 600, 1000, 1500, 2000, 2500, and up to 3000 grits.

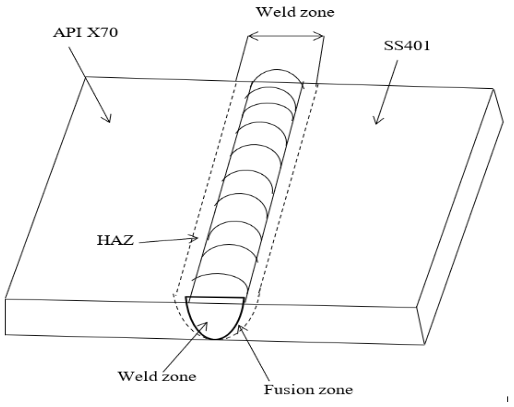

Fig. 1. Schematic representation of the dissimilar weld joint between API X70 and SS 410.

Welding Parameters

Parameter	HI-1	HI-2
Current (A)	116	100
Voltage (V)	20	16
Welding Speed (mm/sec)	3.166	3.102
Heat input (kJ/mm)	0.814	0.573

Final polishing was carried out using alumina powders (grades 1, 2, and 3) on wall-wet paper to obtain a mirror-like finish. Etching was subsequently performed to expose the internal grain structure of the specimens. For API X70 steel, Nital prepared by mixing 1 mL of nitric acid (HNO_3) with 99 mL of ethanol to reveal the ferritic and martensitic microstructures common in low-carbon steels. In the case of SS 401 stainless steel, etching was done using a 10% oxalic acid solution, made by dissolving 10 grams of oxalic acid in 90 mL of reagent-grade water. This etchant is effective for visualizing grain boundaries in corrosion-resistant stainless steels. Microstructural examination of the specimens was conducted using an optical microscope equipped with objective lenses ranging from 5x to 100x magnification. Optical microscopy was used to assess grain size, phase distribution, and surface irregularities. All procedures conformed to ASTM E3, ASTM E407, and ISO 17639 standards to ensure the reliability and reproducibility of results. The fracture surfaces of welded samples underwent fractographic analysis using SEM at different magnification levels between 500x, 1000x, and 2000x up to 2500x. The high-resolution imaging system permitted researchers to examine fracture conditions and weld faults in addition to the behaviour of stressed materials. The ASTM E1508 standard guided how the SEM analysis was performed to achieve accurate results for weld quality evaluation together with material integrity checks. Only 26.5 g of sodium chloride with 4 g of magnesium sulphate and 1 g of calcium chloride and 0.2 g of sodium bicarbonate had to be dissolved into one liter of distilled water for creating the seawater solution. Acidified hydrochloric acid served to adjust the pH of the mixture until it reached 8.2. Separately, a sodium thiosulfate solution was formulated by dissolving 24.81 g of sodium thiosulfate in one litre of distilled water, with the pH adjusted to 3 through the addition of hydrochloric acid. These chemical environments are commonly utilized in corrosion studies, controlled reaction experiments, or research that requires precise ionic conditions and pH control. The experimental procedure involved immersing specimens made of API X70, SS 401, and their respective welded samples (produced under HI-1 and HI-2 conditions) in the prepared solutions for a duration of 48 days. At regular intervals of four days, the samples were removed, thoroughly dried, and weighed using a precision balance to record weight changes accurately. Each material group included four specimens: two immersed in the seawater solution and two in the sodium thiosulfate solution. The approximate dimensions of the specimens were 30 mm in length, 15 mm in width, and 12 mm in thickness. This methodical approach allowed for consistent data collection and a reliable assessment of the corrosion rates and degradation patterns under different chemical exposures. The corrosion rate was determined as:

$$\text{Corrosion Rate}=(8.75\times10^{4}\times\text{Weight Loss in mg})/\ (\text{Density}\times\text{Surface Area}\times\text{Exposure Time in days}). \qquad (2)$$

This formula incorporates the weight loss of the specimen, its surface area, density, and the total duration of exposure, ensuring accurate quantification of material deterioration in simulated corrosive environments.

II. Results and Discussion

2.1. Microstructure Analysis

Figure 2 shows microstructure of API X70 and SS 401 steel samples, revealing how their microstructures evolve across different welding zones: base metal (BM), weld metal, and the heat-affected zone (HAZ)-when subjected to two distinct levels of heat input: HI-1 (higher) and HI-2 (lower).

Each image was captured at a magnification of 500×, and key microstructural features such as ferrite, pearlite, bainite, and martensite-austenite (MA) are clearly identified. In the BM region, API X70 displays the expected mixture of ferrite and pearlite, typical of this type of pipeline steel. On the other hand, the SS 401 sample contains ferrite along with MA phases, reflecting the duplex or semi-martensitic nature of some stainless steels. The weld metal zones created with higher heat input (HI-1) exhibit a combination of pearlite, ferrite, and MA (Martensite-austenite) (as seen in Figure 2c), while those formed under lower heat input (HI-2) still include ferrite and MA, though with noticeable differences in grain morphology (Figure 2d). A particularly interesting and unconventional finding appears in the HAZ. For both steels, especially SS 401, finer grains are seen under HI-1 (Figures 2e and 2f), while coarser grains emerge under HI-2 (Figures 2g and 2h). This outcome runs contrary to the general assumption that higher heat input usually results in larger grains due to slower cooling, and lower input leads to finer structures owing to quicker thermal cycles. This reversal in grain behaviour may be attributed to complex thermal phenomena. In lower heat input conditions, faster travel speeds and more localized heating can generate steep thermal gradients, which, in certain alloys like SS 401, can trigger abnormal grain growth. The time spent at elevated temperatures, even if shorter, may still be sufficient to promote grain coarsening, especially in metals sensitive to thermal shock or with specific phase transformation characteristics [17-19]. To summarize, this microsturure study reveals that grain structure is influenced not just by the level of heat input but by a combination of thermal cycle dynamics and the intrinsic properties of the materials involved. These results highlight the need for a more nuanced approach when predicting weld microstructures.

2.2. Visual Examination of Corroded Specimens

Figure 3 shows the corrosion behavior of specimens exposed to seawater and sodium thiosulphate environments over different duration of 8, 16, 32, and 48 days.

The tested materials included base metals (API X70 and SS401) and welded interface zones formed under different heat inputs (HI-1 and HI-2). The visual appearance of corrosion products varied distinctly with both time and environment. In the seawater environment, the API X70 base metal initially developed light brown rust patches, indicative of early oxide formation. Over

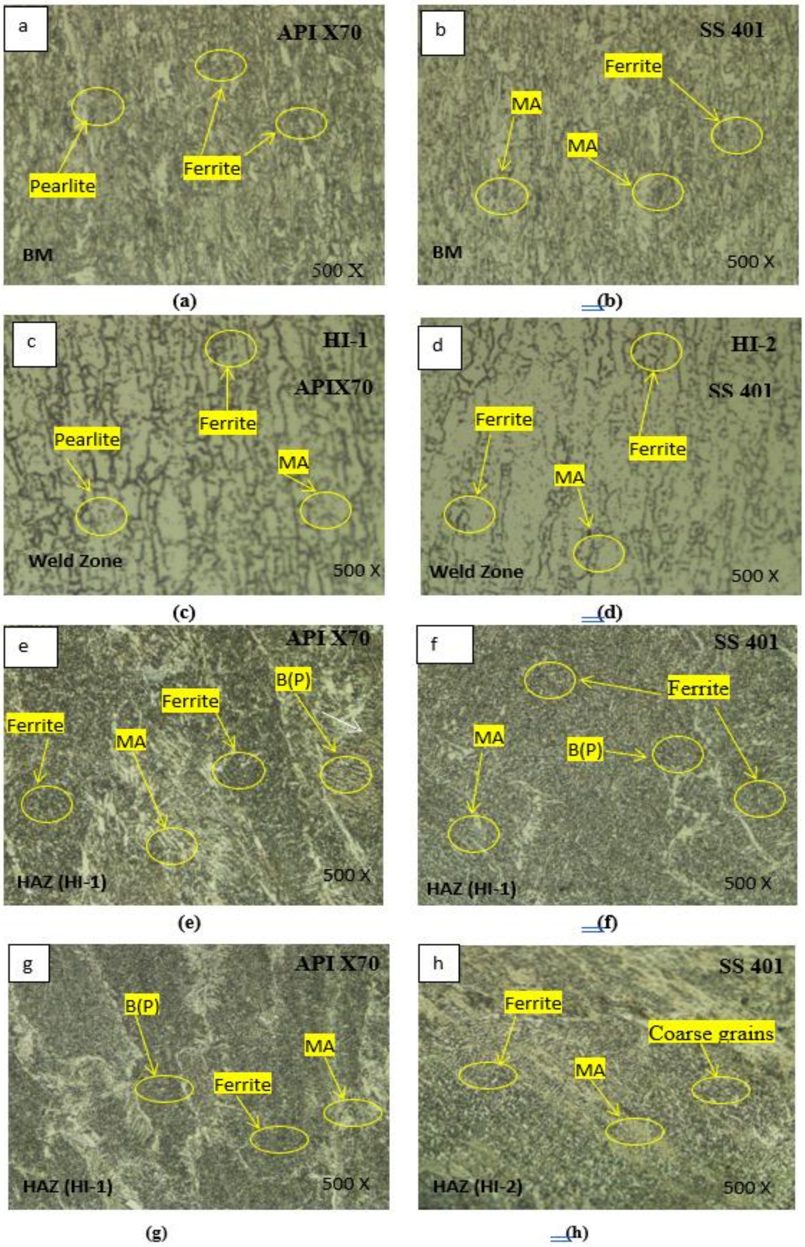

(a) (b) (c) (d) (e) (f) (g) (h)

Fig. 2. Microstructure of (a) API X70, (b) Stainless steel (SS 401), (c) Heat input (HI-1), (d) Heat input (HI-2), (e) HAZ (HI-1) of API X70, (f) HAZ (HI-1) of SS 401, (g) HAZ (HI-2) of API X70, HAZ (HI-2) of SS 401of stainless steel (SS401), All images at 500 magnification (500 X) Note: HI-1: Weld fabricated at Higher Heat input 1; HI-2: Weld fabricated at Lower Heat input 2.

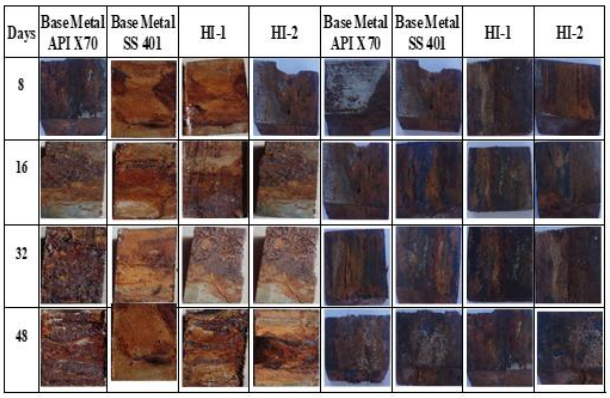

Fig. 3. Visual inspections of test specimens in sea water and sodium thiosulphate solutions.

time, these evolved into darker, flaky layers, suggesting progressive oxidation and surface deterioration. In contrast, the SS401 base metal exhibited more uniform corrosion, with a gradual colour shift from brown to darker shades, likely due to the formation of a stable passive layer. The HI zones, particularly HI-2, revealed significant surface degradation, marked by irregular patches of dark brown to black corrosion products, highlighting their increased susceptibility to localized attack in the weld and heat-affected zones. Under sodium thiosulphate exposure, the corrosion severity increased substantially. API X70 surfaces darkened rapidly, forming thick black scales during extended immersion: characteristic of sulfide corrosion, possibly iron sulfide formation [20]. SS401 also showed discoloration, though to a slightly lesser extent. The HI zones, especially HI-1, experienced extensive corrosion, including the appearance of dense black layers and white crystalline residues. These features suggest aggressive localized corrosion phenomena, such as pitting or crevice corrosion, promoted by thiosulphate ions. Across both corrosive environments, the colour transformation of corrosion products– from light brown to dark brown, black, and white – visually represented the extent and nature of degradation [21]. Welded interface zones (HI-1 and HI-2) consistently exhibited greater deterioration, attributed to their metallurgical heterogeneity and potential galvanic interactions. These visual assessments align with mass loss and corrosion rate measurements, confirming that welded joints, particularly at dissimilar metal interfaces, are more prone to degradation in harsh environments.

2.3. Weight loss study analysis

Figures 4 and 5 illustrate how different metallic specimens namely API X70, SS 401, and their welded counterparts (HI-1 and HI-2)- respond to corrosive exposure in two distinct environments: natural-like sea-water and sodium thiosulphate solution, across a 48-day immersion period. In seawater conditions (Figure 4a), all specimens show a progressive decrease in weight, indicating material degradation. Among the materials tested, SS 401 consistently demonstrates the lowest percentage of weight loss. This performance is attributed to its chromium-rich composition, which enables the development of a protective passive film on the surface, impeding corrosion progression. API X70 experiences slightly higher losses, reflecting a moderate resistance level. However, the weld zones of HI-1 and particularly HI-2-display the highest degradation. Under sodium thiosulphate exposure (Figure 4b), degradation is significantly more aggressive. Weight loss progresses more rapidly across all sample types when compared to seawater immersion. SS 401, while still performing better than the rest, shows a compromised protective response in the sulfide-rich medium. API X70 fares worse in this solution, and the welded joints-particularly HI-1-exhibit the greatest mass loss, nearing -0.18% by day 48.

The strong reactivity of thiosulphate with metal surfaces likely promotes intense pitting and crevice corrosion, especially in the heterogeneous weld zones where electrochemical potentials vary locally. In seawater (Figure 5a), SS 401 again demonstrates superior resistance, with the lowest recorded corrosion rate, close to 0.75 mm/year. API X70 shows moderate deterioration (~1.6 mm/year), while the weld zones register the highest corrosion rates, with HI-2 reaching approximately 2 mm/year. When examined in the sodium thiosulphate environment (Figure 5b), corrosion rates intensify for all specimens. HI-1 emerges as the most severely affected, with a rate exceeding 2.1 mm/year which may not effectively resist aggressive ionic attack in sulfide-rich solutions. SS 401 retains the lowest corrosion rate in this environment as well (~0.9 mm/year), while API X70 and HI-2 experience intermediate levels of deterioration. Welded joints, particularly those with high heat input, are most vulnerable, while SS 401 consistently shows the best resistance across both environments. This underscores the importance of optimized welding processes and material selection in corrosive service applications to ensure

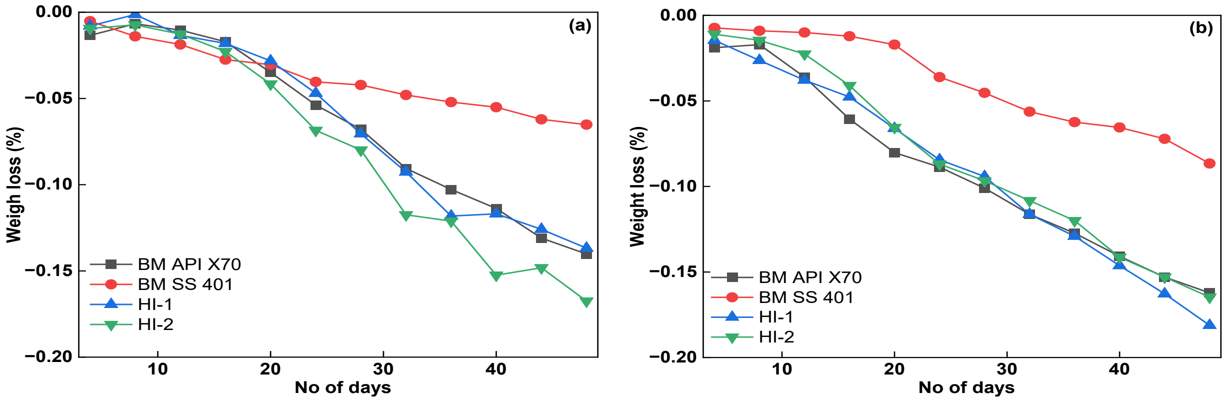

Fig. 4. Weigh loss (%) of base metal (API X70, SS 401) and heat-input weld zone (HI-1, HI-2), immersed in (a) sea water and (b) Sodium thiosulphate solution for 48 days.

structural longevity.

2.4. Fractography Analysis

The SEM analysis reveals distinct morphological features across various weld zones under differing heat inputs. In the fusion zone (FZ), the low heat input condition (HI-1) (Figure 6a) produces a fracture surface rich in fine fibrous dimples, which is indicative of significant plastic deformation and a predominantly ductile failure mechanism. Conversely, the FZ under lower heat input (HI-2) (Figure 6b) displays deeper and more pronounced dimples, suggesting coarser microstructures and a possible reduction in fracture toughness due to grain growth and softening. On the API X70 side of the heat-affected zone (HAZ), fracture behavior undergoes a notable transformation with changes in thermal exposure. The HI-1 condition (Figure 6c) results in a mix of deep dimples and irregular cleavage patterns, pointing to a combination of ductile and semi-brittle failure. Under the HI-2 condition (Figure 6d), however, the morphology becomes more cleavage-dominant with fewer dimples, implying a shift towards brittle fracture behavior. This alteration is likely associated with increased formation of martensitic or mixed microstructures under prolonged thermal cycling [22]. The SS 401 HAZ shows less dramatic changes

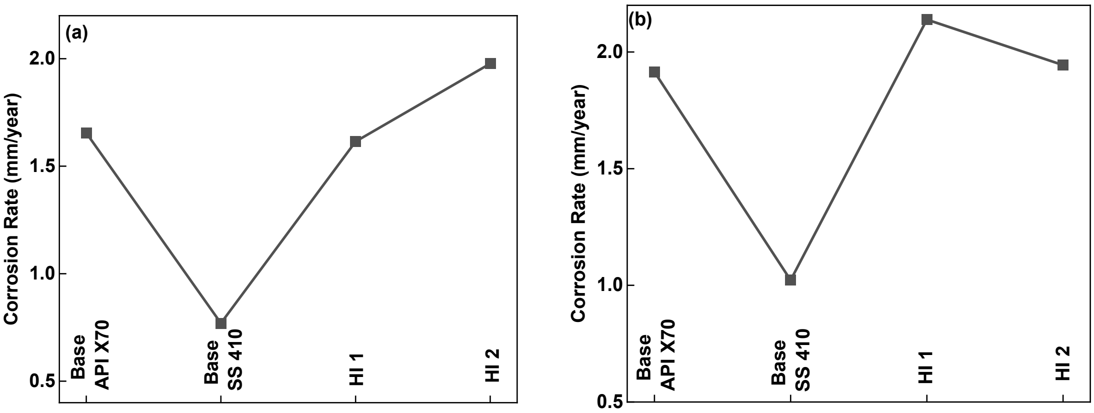

Fig. 5. Corrosion rate of base metal (API X70, SS 401) and heat-input weld zone (HI-1, HI-2), immersed in (a) sea water and (b) Sodium thiosulphate solution for 48 days.

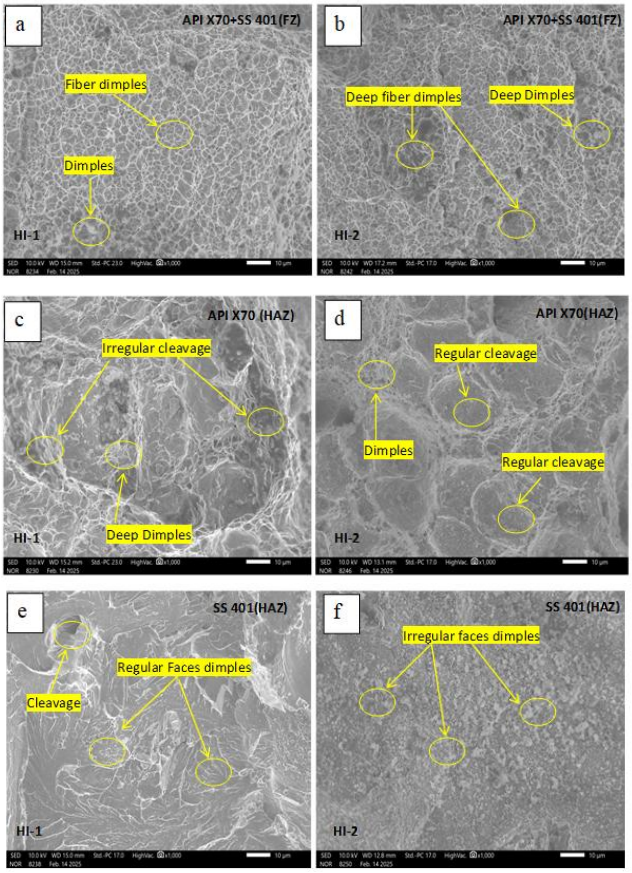

Fig. 6. SEM analysis of API X70+ SS 401 MIG weld joint Fusion Zone alloy (FZ) HI-1, (b) FZ API X70+ SS 401 HI-2, (c) HAZ alloy API X70 side HI-1, (d) HAZ alloy API X70 side HI-2, (e) HAZ alloy SS 401 side HI-1, (f) HAZ alloy SS 401 side HI-2.

between HI-1 and HI-2. In the HI-1 condition (Figure 6e), the presence of regular cleavage and some dimples suggests a brittle-to-semi-ductile fracture mode. Under HI-2 (Figure 6f), irregularly shaped dimples become more apparent, although the overall appearance still leans towards limited ductility, reflecting the inherent nature of the stainless-steel microstructure. Correlating these microstructural observations with impact energy values from Charpy testing provides additional clarity. The API X70 HAZ under HI-1 demonstrates the highest impact energy at 298 J, supporting the dominance of ductile behavior seen in the SEM analysis. This value falls drastically to 120 J under HI-2, underscoring the negative impact of excessive heat input on the mechanical integrity of this region. The FZ, in contrast, shows an improvement in impact energy from 154 J (HI-1) to 196 J (HI-2), likely due to better homogenization in the weld metal, though this comes at the cost of HAZ toughness. In the SS 401 HAZ, impact energy values remain relatively steady at 172 J and 160 J for HI-1 and HI-2, respectively, echoing the consistent brittle features observed microscopically. These values confirm that SS 401, though stable in fracture morphology, exhibits comparatively lower energy absorption regardless of heat input variation.

2.5. Hardness Test Results

The hardness profile across the dissimilar weld between API X70 and SS 401 for two different heat input conditions (HI-1 and HI-2) as shown in Figure 7 reveals clear distinctions in the mechanical response of the welded regions, highlighting the influence of thermal input during the MIG welding process. The fusion zone (centre of the weld) consistently displays the highest hardness values in both heat input conditions. Specifically, under HI-1, the Vickers hardness (VHN) within the fusion zone remains relatively stable around 380 HV, whereas in HI-2, it is slightly lower, averaging near 365 HV. This difference may be attributed to grain coarsening and softening effects which reduces the extent of solid-solution strengthening and microstructural refinement. Moving away from the weld centre toward the heat-affected zones (HAZ) on both sides, a sharp drop in hardness is observed [22-23]. For HI-1, the decrease is more abrupt, particularly on the API X70 side (left side of the graph), where the hardness falls to approximately 300 HV. A similar trend is seen on the SS 401 side (right side), where the values drop below 270 HV. The distinct dip in hardness near the fusion boundary can be associated with thermal softening and possible tempering effects, especially in the coarse-grained HAZ. Comparatively, the HI-2 profile shows a more gradual transition but overall lower hardness values in the HAZ regions, ranging from 260–300 HV. This reduction implies a more pronounced thermal effect during welding, likely promoting microstructural degradation and reduced dislocation density. Beyond the HAZ, in the unaffected base metal regions on both sides of the weld, the hardness stabilizes again. The base metal hardness for API X70 (left region beyond –4 mm) remains around 310 HV for both conditions, while the SS 401 side (beyond +4 mm) is slightly lower, close to 270 HV. These reference values derive from base alloy properties to monitor property change during welding operations. The hardness analysis demonstrates that dissimilar material joints achieve maximum hardness retention through the utilization of HI-2 heat inputs. Under HI-1 the fusion zone exhibits increased hardness as well as distinct heat-affected zone boundaries which indicate refined microstructures with beneficial effects on weld integrity and mechanical strength of dissimilar material joins. Figure 1 shows a schematic diagram of the different welding connections between the API X70 and SS401. This diagram shows the welding zones that include both the fusion zone and the heat zone (HAZ). In the merger zone, the basic materials of API X70 and SS401 melted and melted and fused during the welding process. The HAZ next to the fusion zone is the area where the heat from the weld seams affected the material structure without actually melting. This scheme visually understands important areas of welding and affects the overall performance of the joints in terms of mechanical and corrosion properties.

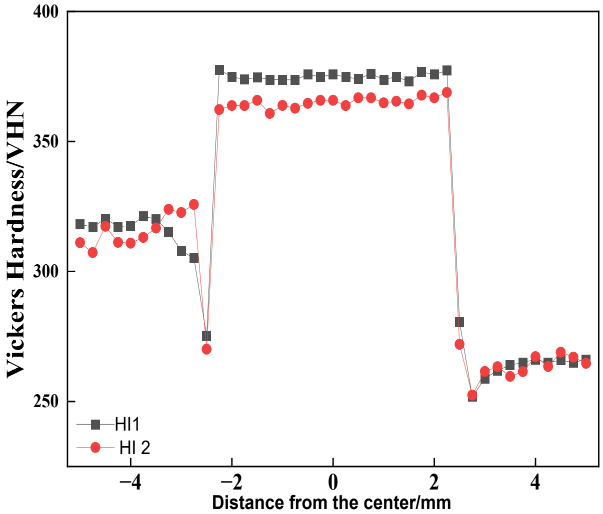

Fig. 7. Hardness variation across the dissimilar weld for HI-1 an HI-2.

The microstructure of API X70 and SS 401 at various heat input values is shown in Figure 2 below. The indicated micrographs (a)–(h) demonstrate different microstructure like pearlite, ferrite, martensite-austenite (MA) phases, and distribution of grains under various heat input conditions. (a) and (b), respectively, represent the base metal (BM) of API X70 and SS 401. The API X70 consists of pearlite and ferrite and the SS 401 has ferrite and MA Phases. (c) and (d) also show hot pipe zones 1 and 2, at higher and lower heat inputsond) HI-1 and HI-2, respectively, with different microstructural features such as ferrite and MA phases. (e) and (f) emphasize the HAZ of API X70 and SS 401 under HI-1 showing abundance of MA phase in the both base metals. having ferrite content in API X70. (g) and (h) compare the microstructures of both API X70 and SS 401 HAZs under HI-2 show more coarser grains in SS 401, and or ferrite and MA phases present in both materials. This figure displays the profound impact that the heat input during welding has on the occurrence and growth of various phases and grains in dissimilar joints and thus on the mechanical and corrosion behaviour.

$$(HI = \eta HVI/S)$$

Table 1.

Chemical composition (in wt.%) of base metals API X70 and Stainless Steel 410 (SS 401) as per PSL1 specifications

Element	Carbon (C)	Manganese (Mn)	Silicon (Si)	Phosphorus (P)	Sulfur (S)	Chromium (Cr)	Nickel (Ni)
API X70 (max %) (PSL1)	0.28	1.40	0.55	0.03	0.03	–	–
Stainless steel 401 (%) (PSL1)	0.032	1	1	0.04	0.03	11.54	0.25

Table 2.

Mass (in grams) over time for base metals (API X70 and SS 401) and weld interface zones (HI-1 and HI-2) in seawater and sodium thiosulphate environment

Mass loss								
Seawater					Sodium thio sulphate			
No of days	Base metal (API X70)	Base metal (SS401)	HI-1	HI-2	Base metal (API X70)	Base metal (SS401)	HI-1	HI-2
0	42.12	42.12	42.12	42.12	42.12	42.12	42.12	42.12
4	42.1066	42.1148	42.112	42.1106	42.1011	42.1127	42.1054	42.109
8	42.1133	42.106	42.1187	42.1127	42.1029	42.111	42.0937	42.1054
12	42.1096	42.1013	42.1066	42.1073	42.0839	42.11	42.0821	42.0974
16	42.1029	42.0925	42.1019	42.0972	42.0594	42.1078	42.0723	42.079
20	42.0851	42.0896	42.0918	42.0784	42.0398	42.1029	42.0539	42.0545
24	42.0662	42.0796	42.073	42.0515	42.0313	42.0839	42.0356	42.0331
28	42.0521	42.0778	42.0495	42.0401	42.019	42.0747	42.0258	42.0233
32	42.0294	42.072	42.0273	42.0025	42.0037	42.0637	42.0037	42.0117
36	42.0172	42.0679	42.0018	41.9989	41.9927	42.0576	41.9909	42
40	42.0062	42.0649	42.0031	41.9675	41.9792	42.0545	41.9737	41.9786
44	41.989	42.0579	41.9941	41.9718	41.967	42.0478	41.9572	41.967
48	41.9798	42.0548	41.9832	41.9525	41.9578	42.0334	41.9388	41.9553

Figure 3 presents a visual inspection of the test sample. These are exposed to seawater and sodium thiosulfate for various periods (8, 16, 32, 48 days). The image in the figure shows the corrosion behavior of both the base metals, API X70 and SS 401, as well as weld compounds produced under higher and lower thermal input conditions (Hi-1 and Hi-2). The API X70 exhibits significant corrosion, especially with longer exposure times, while the SS 401 improves performance thanks to its passive film rich in protective chromium.The following four columns show the corrosion behavior of weld connections under Hi-1 and Hi-2 conditions. High-temperature weld seams (HI-1) exhibit more corrosion than low-heat welding (HI-2) especially after longer exposure times. This highlights the effect of thermal input on corrosion resistance, which in turn provides better protection for Hi-2.

In Figure 4, weight loss (%) of base metal (API X70 and SS 401) and heated welding zones (Hi-1 and Hi-2) are applied to two different exposure environments: seawater (panel A) and sodium thiosulfate solution (plate B). Weight loss is pursued over 48 days. Panel (a) shows weight loss in seawater. This results in the API X70 has the highest corrosion rate, especially in the Hi-1 welding zone, followed by the SS 401. The Hi-2 welding zone is an API X70 welding zone, based on better corrosion resistance, with results from API X70 and SS 401. SSS-401-LSS-401-. Sodium-thiosulfuric acid solution. Like seawater, the API X70 has more corrosion compared to the SS 401. The Hi-1 welding zone again shows a higher weight loss rate, but the Hi-2 weld seams in this environment also violate corrosion resistance over time.

In Figure 5, the corrosion rate (in mm/year) of the base metal (API X70 and SS 401) and the heat-input weld zones (HI-1 and HI-2) are shown for both seawater (panel a) and sodium thiosulphate solution (panel b) after 48 days of exposure. Panel (a) shows that SS 401 has the lowest corrosion rate, particularly in the HI-2 weld zone, which demonstrates the best corrosion resistance. On the other hand, API X70 experiences a significantly higher corrosion rate, especially in the HI-1 weld zone. Panel (b) illustrates similar findings in the sodium thiosulphate solution, where SS 401 again exhibits the lowest corrosion rate, and API X70, particularly in the HI-1 weld zone, shows the highest corrosion degradation. These results reinforce the observation that lower heat input (HI-2) provides better corrosion resistance for both base materials, with SS 401 performing better overall.

In Figure 6, the Scanning Electron Microscopy (SEM) analysis of the MIG welded joint between API X70 and SS 401 is presented, highlighting the microstructural features in both the Fusion Zone (FZ) and Heat-Affected Zone (HAZ) under different heat input conditions (HI-1 and HI-2). Panels (a) and (b) show the fusion zone of the API X70 + SS 401 joint under higher heat input (HI-1) and lower heat input (HI-2), respectively. In HI-1, the fusion zone exhibits fiber dimples and dimples, whereas in HI-2, deeper fiber dimples and deep dimples are observed, indicating differences in the material's fracture surface due to the heat input. Panels (c) and (d) focus on the HAZ of

API X70 on either side of the weld under HI-1 and HI-2, showing irregular cleavage and deep dimples in HI-1, while the HI-2 side shows more regular cleavage and dimples. Panels (e) and (f) show the HAZ of SS 401, with panel (e) under HI-1 displaying regular faces dimples and cleavage, and panel (f) under HI-2 showing irregular faces dimples.This figure provides insights into the fracture mechanisms in both the fusion and heat-affected zones, revealing how the heat input affects the material's fracture surface morphology. The presence of dimples and cleavage regions suggests a relationship between the welding conditions and the mechanical properties of the joint.

Table 3.

Charpy impact test results (in Joules) for different regions of the dissimilar welded joint between API X70 and SS 401.

Specimen	Materia Name	Impact-test result (J)
1	API-X70+SS401 (FZ, HI-1)	154
2	API-X70 (HAZ, HI-1)	298
3	SS 401 (HAZ, HI-1)	172
4	API-X70+SS401 (FZ, HI-2)	196
5	API-X70 (HAZ, HI-2)	120
6	SS 401 (HAZ, HI-2)	160

Vickers hardness variation across dissimilar weld is plotted in Figure 7 for higher heat input condition HI-1 and lower heat input condition HI-2. Hardness distribution along a line from weld center outward toward edges measured in millimeters is graphically represented with varying intensity. HI-1 conditions represented by square markers exhibits significant hardness peak near weld center indicating hardening effect deeply within fusion zone. Hardness decreases sharply towards heat-affected zones and then stabilizes somewhat erratically as it moves further away from center. HI-2 conditions denoted by circular markers exhibits hardness peak in fusion zone but overall hardness remains significantly lower than that of HI-1. Hardness decline proceeds rather gradually suggesting somewhat uniform distribution across weld and heat affected zone. Higher heat input HI-1 yields more pronounced hardness variation across weld compared to lower heat input HI-2 highlighting effect quite vividly.

Conclusion

The present work was focused on the dissimilar welding of API X70 pipeline steel and SS 401 ferritic stainless steel by Metal Inert Gas (MIG) welding process. The research investigated microstructural changes, mechanical properties and corrosion behaviour with fractographic characteristics of in the weld joints. The results indicate that when suitable parameters employed, MIG welding can be carried out to manufacture sound joints of these dissimilar metals. Microstructural observations revealed distinct differences across the weldment zones. API X70 exhibited a typical ferrite-pearlite structure, while SS 401 showed a fully ferritic matrix. The heat-affected zones (HAZ) of both metals displayed grain growth or refinement depending on proximity to the fusion line. The fusion zone (FZ) showed a dendritic structure, influenced by the mixing of alloying elements and rapid solidification during welding. This heterogeneous microstructure affected both mechanical performance and corrosion resistance. Microhardness testing showed variation across the weldment, with the fusion zone displaying the highest hardness values due to rapid cooling and possible formation of hard phases. The HAZ of API X70 had reduced hardness, likely from grain coarsening, while the HAZ of SS 401 showed a slight increase in hardness due to grain refinement. These localized changes in hardness are critical for assessing joint integrity under load. Corrosion testing in sea water solution revealed that SS 401 had superior corrosion resistance, followed by API X70. The fusion zone exhibited the poorest corrosion resistance, attributed to the compositional mismatch and microstructural heterogeneity, which promotes galvanic activity. Fractographic analysis of fractured impact specimens showed a mixture of ductile and brittle features, with the fracture typically initiating in the fusion zone.

***Sharma Lochan* –** PhD**,** Associate Professor;
Jakhar Amman – PhD, Assistant Professor;
Sharma Kanika – Assistant Professor;
***Singh Mukhtiar* -** PhD, Professor;
***Singh Mandeep Rayat* –** Assistant Professor;
***Mariia Liaskovska* –** Assistant Professor;
***Abaszade Rashad* –** PhD, Associate Professor.

[1] S. Liu, Y. Zhang, H. Li, X. Wang, *Weldability of API 5L X70 steel under submerged arc welding conditions*, Journal of Manufacturing Processes, 28, 560 (2017); https://doi.org/10.1016/j.jmapro.2017.07.016.

[2] W. D. Callister, Materials science and engineering: An introduction, 7th ed., Wiley, New York (2007).

[3] H. Yang, L. Zhang, Y. Li, Q. Chen, *Corrosion inhibition in API 5L X70 steel using rare earth compounds*, Corrosion Science, 182, 109278 (2021); https://doi.org/10.1016/j.corsci.2020.109278.

[4] A. Singh, R. K. Singh, S. Das, *Hydrogen embrittlement susceptibility in API 5L X70 steel: Effects of microstructure and cold rolling*, Journal of Materials Research and Technology, 9(5), 10456 (2020); https://doi.org/10.1016/j.jmrt.2020.07.053.

[5] J. W. Park, S. H. Lee, Y. M. Kim, *Microstructure evolution during thermomechanical controlled processing of API 5L X70 steel,* Materials Science Forum, 980, 55 (2019); https://doi.org/10.4028/www.scientific.net/MSF.980.55.

[6] S. Kou Welding metallurgy, 2nd ed., Wiley-Interscience, Hoboken, NJ (2003).

[7] American Welding Society Dissimilar metal welding guidelines, AWS, Miami, FL (n.d.).

[8] J. C. Lippold, D. J. Kotecki, *Welding metallurgy and weldability of stainless steels*, Wiley-Interscience, Hoboken, NJ (2005).

[9] ASM International ASM Handbook, Volume 6: Welding, Brazing, and Soldering, ASM International, Materials Park, OH (1993).

[10] R. S. Mishra, M. W. Mahoney, *Friction stir welding and processing*, ASM International, Materials Park, OH (2007).

[11] STM International ASTM E8/E8M-21: Standard test methods for tension testing of metallic materials, ASTM International, West Conshohocken, PA (2021); https://doi.org/10.1520/E0008_E0008M-21

[12] D. H. Kim, S. J. Kim, C. Y. Kang, *Effect of heat input on microstructure and mechanical properties of API 5L X70 pipeline steel welds,* Welding Journal, 94(2), 45s (2015).

[13] Y. Wang, X. Liu, J. Zhang, *Impact of cooling rates on microstructure and mechanical properties in API X70 welds*, Metallurgical and Materials Transactions A, 46(2), 600 (2015); https://doi.org/10.1007/s11661-014-2665-4

[14] J. F. Santos, T. Watanabe, H. Okado, *Optimization of dissimilar welding parameters for API X70 and SS400 using gas metal arc welding*, Journal of Manufacturing Science and Engineering, 135(4), 041009 (2013); https://doi.org/10.1115/1.4024701.

[15] M. Sharma, V. K. Singh, R. Kumar, *Strategies for minimizing cold cracking in API X70 to SS400 weld joints*, Welding International, 32(6), 456 (2018); https://doi.org/10.1080/09507116.2017.1343634.

[16] V. Ramasamy, S. K. Albert, A. K. Bhaduri, *Effect of filler material on mechanical properties of dissimilar welded joints between API X70 and SS400 steels*, Materials & Design, 55, 483 (2014); https://doi.org/10.1016/j.matdes.2013.10.018.

[17] T. Kamal, M. A. Raza, S. A. Hussain,*Mechanical, microstructure, and corrosion characterization of dissimilar austenitic 316L and duplex 2205 stainless-steel ATIG welded joints*, Materials, 15(7), 2470 (2022); https://doi.org/10.3390/ma15072470.

[18] N. Ghosh, S. K. Albert, A. K. Bhaduri, *GMAW dissimilar welding of AISI 409 ferritic stainless steel to AISI 316L austenitic stainless steel by using AISI 308 filler wire*, Engineering Science and Technology, an International Journal, 20, 1334 (2017); https://doi.org/10.1016/j.jestch.2017.05.009.

[19] M. Rahmani, M. K. Besharati-Givi, *Evaluation of microstructure and mechanical properties in dissimilar austenitic/super duplex stainless steel joint,* Journal of Materials Engineering and Performance, 23, 3745 (2014); https://doi.org/10.1007/s11665-014-1153-3.

[20] J. Labanowski, *Stress corrosion cracking susceptibility of dissimilar stainless steels welded joints*, Journal of Achievements in Materials and Manufacturing Engineering, 20, 255 (2007).

[21] L. Peguet, B. Malki, B. Baroux Influence of cold working on the pitting corrosion resistance of stainless steels, Corrosion Science, 49, 1933–1948 (2007); https://doi.org/10.1016/j.corsci.2006.11.010.

[22] S. Jana, *Effect of heat input on the HAZ properties of two duplex stainless steels,* Journal of Materials Processing Technology, 33, 247 (1992); https://doi.org/10.1016/0924-0136(92)90234-6.

[23] J. Verma, V. Taiwade, *A comparative study on the effect of electrode on microstructure and mechanical properties of dissimilar welds of 2205 austeno-ferritic and 316L austenitic stainless steel*, Materials Transactions, 57, 494 (2016); https://doi.org/10.2320/matertrans.M2015403.

Лочан Шарма[1], Амман Джахар[2], Каніка Шарма[3], Мухтіар Сінгх[4],
Мандіп Сінгх Раят[4], Марія Лясковська[5], Рашад Абасзаде[6,7,8,9]

Дослідження мікроструктури, корозії та механічних властивостей з'єднання API X70 і SS401, отриманого методом MIG

[1]Факультет досліджень і розвитку, Університет Чандігарх, Мохалі, Пенджаб, Індія;
[2]Факультет машинобудування, Університет Чандігарх, Мохалі, Пенджаб, Індія;
[3]Факультет комп'ютерних наук та інженерії, Університет Чандігарх, Мохалі, Пенджаб, Індія;
[4]Університет Lovely Professional, Джаландхар - Делі, Grand Trunk Rd, Фагвара, Пенджаб, Індія;
[5]Кафедра біологічної та медичної хімії імені академіка Г.О. Бабенка,
Івано-Франківський національний медичний університет, Івано-Франківськ, Україна;
[6]Кафедра електроніки та автоматики, Азербайджанський державний нафтовий і промисловий університет, Баку, Азербайджан, abaszada@gmail.com;
[7]Кафедра екології, Азербайджанський університет архітектури та будівництва, Баку, Азербайджан;
[8]Кафедра матеріалознавства та технологій нових матеріалів, Ташкентський державний технічний університет імені Іслама Карімова, Ташкент, Узбекистан;
[9]Кафедра електротехніки та електроніки, Міжнародний науково-дослідний інститут «Туран», Баку, Азербайджан

У даному дослідженні для зварювання сталей API X70 та SS 401 використано процес зварювання в середовищі інертного газу (MIG) із застосуванням аустенітного присадного дроту ER309L. Такі з'єднання широко застосовуються в нафтогазовій галузі, де необхідно поєднувати нержавіючу сталь із трубопроводами з високоміцної низьколегованої вуглецевої сталі. Процес MIG-зварювання є економічно ефективним для промислового виготовлення та ремонту завдяки високій продуктивності та швидкості наплавлення. Дослідження спрямоване на вивчення впливу двох рівнів тепловкладення – HI-1 (0,814 кДж/мм) та HI-2 (0,573 кДж/мм) – на мікроструктуру, механічні властивості та корозійну стійкість зварних з'єднань у середовищах модельної морської води та тіосульфату натрію. Мікроструктурний аналіз показав, що менше тепловкладення (HI-2) сприяє формуванню грубозернистої структури та зменшенню частки мартенсит-аустенітної (MA) складової у зоні сплавлення, що забезпечує підвищення ударної в'язкості. Натомість більше тепловкладення (HI-1) призводить до формування дрібнозернистої структури, але супроводжується зростанням крихкості. У зоні термічного впливу (ЗТВ) сталь API X70 демонструє розм'якшення, зумовлене укрупненням зерен, тоді як для SS 401 характерні сенсибілізація та формування MA-фази, що негативно впливає на корозійну стійкість. Дослідження корозії показали вищу стійкість SS 401 порівняно з API X70, з мінімальною швидкістю втрати матеріалу (0,75 мм/рік) у морській воді завдяки захисній пасивній плівці, збагаченій хромом. Водночас різнорідні зварні з'єднання, особливо отримані при HI-1, продемонстрували значне корозійне руйнування (2,1 мм/рік у тіосульфатному середовищі), що пов'язано з мікроструктурною неоднорідністю та гальванічною взаємодією. Результати механічних випробувань показали, що зварні з'єднання, отримані при HI-2, мають вищу ударну в'язкість (196 Дж у зоні сплавлення) порівняно з HI-1 (154 Дж), хоча для зони термічного впливу сталі API X70 при HI-2 спостерігається зниження в'язкості (120 Дж), ймовірно внаслідок термічного розм'якшення. Вимірювання твердості показали максимальні значення поблизу межі сплавлення (~380 HV для зразків HI-1) із помітним розм'якшенням у зоні термічного впливу. Отримані результати свідчать, що оптимізація тепловкладення є ключовим чинником для забезпечення балансу між механічною цілісністю та корозійною стійкістю різнорідних зварних з'єднань.

Ключові слова: зварювання металів, X70, SS401, зона термічного впливу, зона плавлення, корозійна стійкість, мікроструктура, фрактографія.